

Hydrogen Bond Effects: A Strategy for Improving Controllability in Organocatalytic Photoinduced Controlled Radical Polymerization Targeting High Molecular Weight

Ya-Ning Li, Sheng-Ye Zhang, Yang Ma, Yi-Jie Ding, Zhi-Hao Chen, Qiao-Ling Che, Long Qin, Xiu-Li Sun, Xiaohua Liu, Xiaoming Feng,* Zhi-Pan Liu,* Xiao-Yan Wang,* and Yong Tang*



Cite This: *ACS Catal.* 2022, 12, 11606–11614



Read Online

ACCESS |

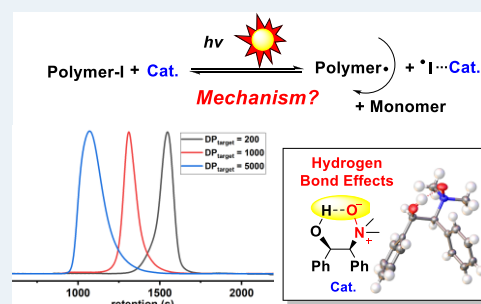
Metrics & More

Article Recommendations

Supporting Information

ABSTRACT: A highly efficacious photoinduced reversible complexation-mediated polymerization (photo-RCMP) system using amino alcohol N-oxide as the catalyst has been developed, allowing access to controlled high-molecular-weight polymers of different methacrylates ($M_n = 497\text{--}815$ kg/mol, $\mathcal{D} < 1.5$), which is very challenging for those known catalytic systems of photo-RCMPs and most organocatalytic photoinduced controlled radical polymerization as it demands higher controllability of catalysts. The monomers can be converted into the polymers nearly quantitatively under simulated or natural sunlight irradiation. Strong hydrogen bond effects are observed in this high-molecular-weight photo-RCMP, in terms of both monomer conversion and molecular weight controllability. The insights of the effects are revealed as the intramolecular hydrogen bond of the N-oxide catalyst modifies the electron density of N-oxide, and thereby facilitates the regeneration of the catalyst (activator) and release of I_2 as a predominant effective regulator of radical concentration, by the studies of X-ray analysis, control experiments, density functional theory calculation, ultraviolet–vis absorption spectroscopy, etc.

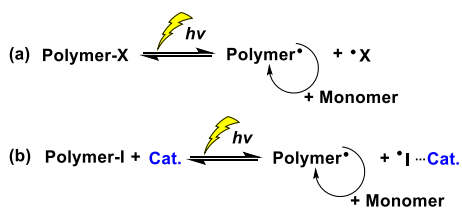
KEYWORDS: organocatalysis, photocatalysis, controlled radical polymerization, high molecular weight, mechanism



INTRODUCTION

Photoinduced controlled radical polymerization (photo-CRP, Scheme 1a), especially the reactions regulated by natural and

Scheme 1. Simplified Mechanism Schematics of (a) Photo-CRP and (b) Photo-RCMP



clean sunlight, is now particularly attractive and promising in practical applications due to its unique advantages including mild conditions, simple operation, few side-reactions, and spatial and temporal control.^{1–15} Thereinto, organocatalytic photo-CRP is more environment-friendly, and emerges as an ideal method for the synthesis of metal-free polymer materials with low toxicity. However, the controllability for organocatalytic photo-CRP is still poor in the cases of achieving high-molecular-weight (M_w) polymers.¹⁶ As the high molecular weights and their distributions of polymers are important in material design for tuning mechanical, thermodynamic, and

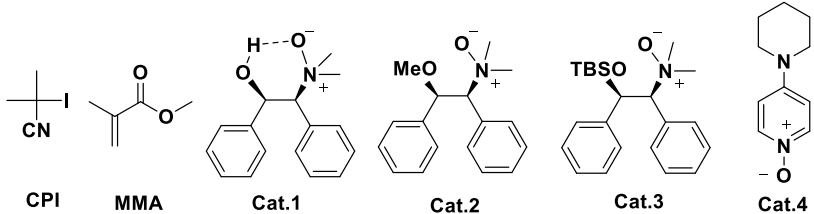
optical properties, many attempts have been done to improve the status and very limited success has been achieved in the past years.^{5,14–19} Elegantly, Goto and later Zhu et al. developed photoinduced reversible complexation-mediated polymerization (photo-RCMP) (Scheme 1b) catalyzed by amines,^{19–21} pyridine N-oxides,¹⁸ carbonyl solvents,²² etc., which emerges as a type of organocatalytic photo-CRP. It has many appealing intrinsic features, such as the use of inexpensive and relatively nontoxic compounds, feasibility over the whole visible region and near-infrared region, and applicability to a range of polymer designs but failed also to give high-molecular-weight polymers with a narrow distribution, which demands higher controllability of catalytic systems.^{18–28} Therefore, it is of great significance to develop novel catalysts to conquer the challenge of achieving high-molecular-weight polymers with narrow M_w distributions via organocatalytic photo-CRP.

Received: July 6, 2022

Revised: August 25, 2022

Published: September 9, 2022



Table 1. Polymerizations of MMA^a


run	Cat.	[Cat.] ₀ /[MMA] ₀	DP _{target}	t (h)	Conv. ^b (%)	M _{n, GPC} (kg/mol)	M _{n, theo} (kg/mol)	Đ
1 ^c	Cat.1	1/400	200	8	67	14.4	13.5	1.18
2	Cat.1	1/400	200	10	97	23.1	19.6	1.32
3 ^d	Cat.1	1/400	200	10	77	22.7	15.6	1.12
4 ^e	Cat.1	1/400	/	10	<1%	/	/	/
5	/	0/400	200	10	<1%	0.573	/	1.15
6	Cat.2	1/400	200	10	10	2.40	2.02	1.27
7	Cat.3	1/400	200	10	80	20.0	16.2	1.17
8	Cat.4	1/400	200	10	90	34.5	18.2	1.27
9 ^f	Cat.1	1/1000	1000	26	97	95.0	97.3	1.28
10 ^f	Cat.1	1/1000	3000	39	99	362	300	1.19
11 ^g	Cat.1	1/1000	5000	39	99	497	496	1.49
12 ^g	Cat.3	1/1000	5000	39	95	781	476	1.70
13 ^g	Cat.4	1/1000	5000	39	67	698	336	2.48

^aUnder simulated sunlight irradiation (using a xenon lamp with an output optical power of 10 W and a wavelength of about 350–900 nm) at ambient temperature, 2-iodo-2-methylpropionitrile (CPI) was used as the initiator, bulk polymerization. ^bMonomer conversion measured by ¹H NMR. ^cUnder natural sunlight exposure. ^dUsing ethyl phenylacetate (EPA) as the solvent, EPA/MMA (v/v, 1/2). ^eWithout an initiator. ^f $f_n(I_2)/n(\text{catalyst}) = 5/100$. ^g $f_n(I_2)/n(\text{catalyst}) = 7.5/100$.

The challenge in synthesizing high-molecular-weight polymers by CRP is the almost inevitable loss of the livingness due to the extremely low concentration of the regulator or deactivator during extended reaction times and iterative initiations. The key to conquering this challenge is to extend the time scale of “living” polymerization via reducing the radical concentration in the polymerization system. As the mechanism studies for RCMP show, the I₂/catalyst complex (I₂⋯Cat.) is one primary deactivator and the system that is more conducive to releasing I₂ exhibits higher polymerization controllability.²⁹ Combining our studies on CRP,^{30–36} we envisioned that facilitating the release of I₂ as another predominant regulator (deactivator) could improve the controllability of photo-RCMP targeting high molecular weight. Thus, we designed Cat.1 with an intramolecular hydrogen bond as it weakens the binding of the N-oxide catalyst to I₂ for our initial study. The N-oxide catalysts derived from amino alcohol could mediate successfully the well-controlled photo-RCMP of various methacrylates and a fluorinated acrylate under simulated or natural sunlight irradiation. More remarkably, we are pleased to find strong hydrogen bond effects in the preparation of high-molecular-weight polymers, in which the molecular weights are still well-controlled (Đ < 1.5) even when M_n is higher than 800 kg/mol, improving the controllability of high-molecular-weight photo-RCMP greatly compared to the known systems. The mechanism involving the hydrogen bond effect is well-studied by X-ray analyses, control experiments, nuclear magnetic resonance (NMR) experiments, ultraviolet (UV)–vis spectrum analyses, and density functional theory (DFT) calculations. Herein, we will report the preliminary results.

RESULTS AND DISCUSSIONS

Design, Synthesis, Application, and Hydrogen Bond Effects of Cat.1 for the Polymerizations of Methyl Methacrylate. It is well known that the intramolecular hydrogen bond between O[−] and active H is very important for the configuration and stability of N-oxides derived from chiral amino acids/alcohols.^{37–40} Obviously, the intramolecular hydrogen bond can tune the electron density of O[−], and thus the complexation of N-oxide with iodine radical, I₂ and alkyl iodide.¹⁸ Thus, it is promising for these N-oxide catalysts to improve the controllability of polymerization by weakening their binding toward I₂ while ensuring a high polymerization rate. Derived from (1R,2S)-2-amino-1,2-diphenylethanol, Cat.1 was conveniently prepared (see Supporting Information) and contains an intramolecular hydrogen bond provided by the hydroxyl group (Table 1). In addition, we also synthesized the N-oxides Cat.2 and Cat.3, which are derived from Cat.1 via protecting the hydroxyl using CH₃I and *t*-butyldimethylchlorosilane, respectively.

Initially, we carried out a bulk polymerization of methyl methacrylate (MMA) targeting the polymerization degree (DP_{target}) as 200 under natural sunlight irradiation ([MMA]₀/[Cat.1]₀/[CPI]₀ = 400/1/2). As shown in Table 1 (run 1), 67% of conversion is achieved without magnetic stirring in 8 h by one working day of sunlight exposure (from 8:30 am to 4:30 pm of October 3rd in Shanghai), with a well-controlled molecular weight (Đ = M_w/M_n = 1.18). In order to facilitate operation and comparison, the other polymerizations were conducted with magnetic stirring under simulated sunlight irradiation using the xenon lamp (with an output optical power of 10 W and a wavelength of about 350–900 nm) at indoor ambient temperature. Cat.1 catalyzes the polymerization efficiently with nearly complete monomer conversion (97%) within 10 h (run 2) and well-controlled molecular weight. The

polymerization using EPA as the solvent ($V_{\text{EPA}}/V_{\text{MMA}} = 1/2$) is also very efficient (run 3), giving a conversion of 77% in 10 h and a well-controlled molecular weight ($\bar{D} = 1.12$). Without an initiator (CPI) or a catalyst, nearly no polymerization takes place under irradiation (runs 4–5). This means that the observed successful photo-RCMP is due to the combination of CPI and N-oxide.

The whole polymerization process up to 97% conversion was tracked (run 2, Table 1). The result shows that the first-order plot of the monomer concentration $[M]$ (Figure 1a) is

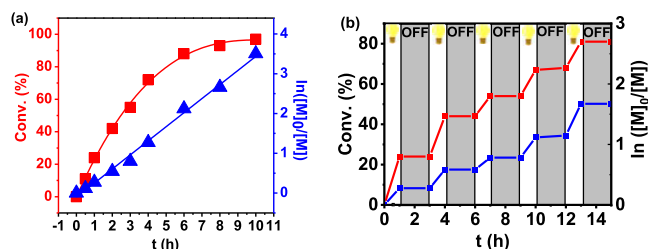


Figure 1. (a) Conversion (red) and $\ln([M]_0/[M])$ (blue) versus time during the whole photo-RCMP (bulk polymerization) process of MMA by Cat.1 (run 2 in Table 1). (b) Conversion (red) and $\ln([M]_0/[M])$ (blue) versus time using Cat.1 during the photo-RCMP of MMA, in which the light was turned on for 1 h and off for 2 h in a repetitive manner for five cycles.

linear. The molecular weight agrees with the theoretical value and the polydispersity index is as small as 1.03–1.32 during the whole process, meaning a sufficiently high frequency of the activation-deactivation cycle (Figure S1a). The detailed experimental data are shown in Supporting Information

(Table S1). Figure 1b shows the excellent temporal control and photoswitchability of the polymerization. Light was turned on for 1 h and off for 2 h in a repetitive manner for five cycles. When the light is turned on, the system is switched “on” and the polymerization smoothly proceeds in all cycles. When the light is turned off, the system is immediately switched “off”, and perfectly no polymerization occurs in the dark. The M_n and dispersity are also well controlled (Figure S1b).

Under the same conditions, Cat.3 can efficiently mediate the polymerization at $DP_{\text{target}} = 200$ (run 7), affording well-controlled molecular weight. By contrast, the conversion by Cat.2 is only 10% in 10 h (run 6). Proton NMR (^1H NMR) measurement revealed that Cat.2 had completely decomposed within about three days after synthesis. Cat.2 is prone to Cope elimination, which occurs through a transition state of a planar five-membered ring (Figure S3).^{41–47} By contrast, about five months after completing all the relevant experiments, the ^1H NMR and mass spectrometry measurements of Cat.3 were conducted and show that the structure was retained during storage. In addition, the structures of Cat.1 and Cat.3 were tracked under the similar conditions of polymerization (under the irradiation of a xenon lamp at $35(\pm 5)$ °C) by ^1H NMR spectra analysis using toluene- d_8 (90%)/acetonitrile- d_3 (10%) as the solvent (a model of MMA medium),¹⁸ and no obvious change was observed in the spectra within 10 h. Probably, it is because that the large steric resistance of its *t*-butyldimethylsilyl-group leads to a high ring tension of the transition state, and thereby the hindered Cope elimination. The best pyridine N-oxide in the literature (4-(piperidin-1-yl)pyridine N-oxide (PPD-PO), Cat.4),¹⁸ was also used for the polymerization of MMA (run 8), giving a monomer conversion of 90% within 10

Table 2. Polymerizations of Various Monomers^a

run	monomer	Cat.	$[\text{Cat.}]_0/[\text{MMA}]_0$	DP_{target}	t (h)	Conv. ^b (%)	$M_{n,\text{GPC}}$ (kg/mol)	$M_{n,\text{theo}}$ (kg/mol)	\bar{D}
1	BMA	Cat.1	1/400	200	10	95	28.4	27.2	1.13
2	LMA	Cat.1	1/400	200	10	73	37.8	37.3	1.18
3	PEGMA	Cat.1	1/400	200	10	99	126	94.2	1.03
4	TFEMA	Cat.1	1/400	200	10	97	31.1	32.8	1.14
5	HFBMA	Cat.1	1/200	100	10	99	26.6	25.0	1.07
6	DMAEMA	Cat.1	1/400	200	10	96	36.2	30.4	1.18
7	HFBA	Cat.1	1/200	100	10	99	21.1	23.6	1.20
8	BzMA	Cat.1	1/400	200	10	98	54.5	34.7	1.35
9	MEMA	Cat.1	1/400	200	10	93	30.8	27.0	1.19
10 ^c	BzMA	Cat.1	1/1000	5000	24	67	652	590	1.42
11 ^d	MEMA	Cat.1	1/1000	5000	24	99	684	714	1.42
12 ^c	BzMA	Cat.3	1/1000	5000	24	26	346	229	1.41
13 ^c	BzMA	Cat.3	1/1000	5000	39	33	697	291	1.68
14 ^d	MEMA	Cat.3	1/1000	5000	24	53	1263	382	1.60
15 ^c	BzMA	Cat.4	1/1000	5000	24	28	2370	247	2.44
16 ^d	MEMA	Cat.4	1/1000	5000	24	28	368	202	1.55

^aUnder simulated sunlight irradiation (using a xenon lamp with an output optical power of 10 W and a wavelength of about 350–900 nm) at ambient temperature, CPI was used as the initiator, bulk polymerization. ^bMonomer conversion measured by ^1H NMR. ^c $n(I_2)/n(\text{catalyst}) = 10/100$. ^d $n(I_2)/n(\text{catalyst}) = 7.5/100$.

h with a narrow M_w distribution ($\mathcal{D} = 1.27$). However, the molecular weight of the polymer is significantly higher than the theoretical value, suggesting that the polymerization by **Cat.4** is less controllable than that by **Cat.1** in such a polymerization. In the work by Goto and co-workers, **Cat.4** (PPD-PO) also efficiently mediated the controlled photo-CMRP of MMA with $DP_{\text{target}} = 200$.¹⁸ The polymerization gave 76% conversion in 11 h, a M_n of 15 kg/mol, and a narrow \mathcal{D} of 1.12, which are not exactly the same as those achieved by **Cat.4** in this work. It should be due to the different polymerization conditions.

Subsequently, we probed the potential of these catalysts in maintaining control over higher molecular weights. Initially, we conducted a range of polymerizations with DP_{target} from 1000 to 5000 by **Cat.1**. As an excellent radical concentration regulator commonly employed in RCMP, a small amount of I_2 was added to increase the deactivation rate and thereby improve the controllability of high-molecular-weight polymerizations. The polymerization of MMA at $DP_{\text{target}} = 1000$ was conducted in the presence of I_2 ($n(I_2)/n(\text{catalyst}) = 0.05$), giving a high conversion of 97% in 26 h, a M_n of 95 kg/mol, and a narrow \mathcal{D} of 1.28 (run 9). The polymerization with the DP_{target} of 3000 is also well controlled, affording 99% conversion in 39 h, a high M_n of 362 kg/mol, and a narrow \mathcal{D} of 1.19 (run 10). Further increasing DP_{target} to 5000 and I_2 dosage ($n(I_2)/n(\text{catalyst}) = 0.075$), the polymerization reaction is still fast and well controlled, affording 99% conversion in 39 h as well as a high M_n of 497 kg/mol, very close to the theoretical value and a relatively narrow \mathcal{D} of 1.49 (run 11). These results are very remarkable, as to the best of our knowledge, organocatalytic photo-CRP has rarely been reported to achieve PMMA with such high and controlled molecular weights,¹⁶ which is very challenging especially for organocatalytic photo-ATRP¹⁷ and photo-RCMP.⁴⁸ By contrast, the polymerization targeting DP as 5000 by **Cat.3** without hydroxyl group gives a molecular weight severely deviating from the theoretical value with a broad M_w distribution ($\mathcal{D} = 1.70$, run 12). The polymerization with a DP_{target} of 5000 by **Cat.4** obtains a much lower conversion of 67% and very poor control over the molecular weight ($\mathcal{D} = 2.48$, run 13). In addition, a much lower conversion and much poorer controllability are observed in the polymerizations of MMA at $DP_{\text{target}} = 5000$ by other reported excellent photo-RCMP catalysts (Table S4), including 1',3',3'-trimethyl-6-nitrospiro[2H-1-benzopyran-2,2'-(2H)-indole] (**Cat.9**), and 1'-diethyl-2,2'-cyanine iodide (**Cat.10**),²¹ compared with those by **Cat.1**. The monomer conversions in 39 h are 13 and 32%, respectively. The molecular weights severely deviate from the theoretical values, and/or the M_w distributions are very broad. These results demonstrate the superiority of **Cat.1** and suggest strong intramolecular hydrogen bond effects in photo-RCMP targeting a high molecular weight.

Scope of Monomers. The polymerization is amenable to a variety of functional methacrylates using **Cat.1**. Table 2 (runs 1–6, 8–9) summarizes the polymerizations of hydrophobic and hydrophilic methacrylates with butyl (BMA), lauryl (LMA), 2,2,2-trifluoroethyl (TFEMA), poly(ethylene glycol) (PEGMA), 2,2,3,4,4,4-hexafluorobutyl methacrylate (HFBMA), (dimethylamino)ethyl (DMAEMA), benzyl (BzMA), and 2-methoxyethyl (MEMA) groups. Low-dispersity ($\mathcal{D} = 1.03$ – 1.35) polymers are obtained with high conversions (mostly >90%) within 10 h in all cases. These results clearly demonstrate the high monomer versatility of **Cat.1**. In

addition, **Cat.1** can efficiently mediate the polymerization of fluorinated acrylate (HFBA), with nearly complete monomer conversion within 10 h and a very narrow M_w distribution ($\mathcal{D} = 1.20$), which might be due to that the electron-withdrawing fluorine atoms facilitate the homolysis of carbon-iodine (run 7). Mediated by **Cat.1**, the polymerizations of BzMA and MEMA with a DP_{target} of 5000 are also efficient and well controlled, affording 67–99% conversions in 24 h as well as a high M_n s of 652–684 kg/mol close to the theoretical values and a narrow \mathcal{D} of 1.42 (runs 10–11).¹⁹ Under the same conditions, **Cat.3**, in the absence of an intramolecular hydrogen bond, gives a much lower conversion in 24 h in the polymerization of BzMA targeting DP as 5000 (run 12) than that by **Cat.1** (26% versus 67%). The conversion only increases to 33% by extending the reaction time to 39 h, and the molecular weight is broadly distributed ($\mathcal{D} = 1.68$). For the polymerization of MEMA, **Cat.3** also yields a much lower conversion (53% versus 99%) and a broader M_w distribution ($\mathcal{D} = 1.60$ versus 1.42). In addition, the molecular weight obtained by **Cat.3** is far from the theoretical value. The best pyridine N-oxide (**Cat.4**),¹⁸ was also used for the polymerizations of BzMA and MEMA with a DP_{target} of 5000. Much like **Cat.3**, the polymerizations by **Cat.4** obtain much lower conversions of 28% and very poor control over molecular weights (runs 15–16). These results further suggest that intramolecular hydrogen bond effects exist in the high-molecular-weight photo-RCMP of different monomers.

Insights into the Effects of the Intramolecular Hydrogen Bond and the Superiority of Cat.1. Evidence of the Intramolecular Hydrogen Bond. The polymerization results by **Cat.1** versus those by **Cat.3** and **Cat.4** suggest that the intramolecular hydrogen bond of **Cat.1** might be key to its superiority in synthesizing high-molecular-weight polymers. In order to get insights into the effects of the intramolecular hydrogen bond, X-ray analysis was conducted, which shows the hydrogen bond between $-\text{OH}$ and O^- in **Cat.1** with the $\text{H}\cdots\text{O}$ distance of 1.81 Å (Figure 2). In addition, during the

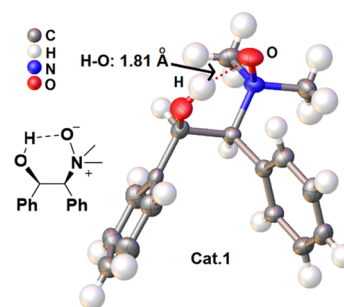


Figure 2. Structure of **Cat.1**.

polymerization process calculated by DFT, such an intramolecular hydrogen bond exists in the optimized structures of the complexes, including $I_2\cdots\text{Cat.1}$ and $I\cdots\text{Cat.1}$, as well as other intermediates involving **Cat.1** (see Supporting Information). In the ^1H NMR spectrum, the chemical signal of $-\text{OH}$ in **Cat.1** is located in a lower field (around 8.4 ppm), compared with that (around 3.5 ppm) of its precursor before oxidation ((1R,2S)-2-(dimethylamino)-1,2-diphenylethan-1-ol) (Figure S10), indicating the existence of hydrogen bonding between $-\text{OH}$ with O^- .⁴⁹ For further confirmation, we performed infrared (IR) spectrometry analysis for **Cat.1** and its precursor. The $\text{O}-\text{H}$ stretch band for the precursor is sharp

around 3500 cm^{-1} when no $\text{O}\cdots\text{H}\cdots\text{O}^-$ bonding is present (Figure S11), while the IR spectrum of **Cat.1** shows a smooth absorption peak around 3416 cm^{-1} , further supporting the intramolecular hydrogen bonding (Figure S11).⁵⁰

Slower Radical Generation Due to the Intramolecular Hydrogen Bond. A radical trap experiment was performed using toluene- d_8 (90%)/acetonitrile- d_3 (10%) as the solvent (a model of the MMA medium),¹⁸ in which we irradiated CPI (80 mM) and 2,2,6,6-tetramethylpiperidine-1-oxyl (TEMPO, 120 mM) as a radical trap with or without a catalyst (40 mM). Figures S4, S6, and S7 show the ^1H NMR spectra of the reaction mixture. After 1 h, new peaks appear and match those of the pure CP-TEMPO independently prepared. Without **Cat.1**, CPI could dissociate to produce radicals with the conversions of 18, 54, and 70% in 1, 2, and 3 h, respectively, while higher corresponding conversions of 34, 83, and 98% are observed in the presence of **Cat.1**, demonstrating that **Cat.1** promotes the dissociation of $\text{R}\text{--}\text{I}$ to generate the alkyl radical. In addition, the radical trap experiment shows that 49% of CPI dissociate to produce radicals in 1 h by **Cat.3**, which is higher than that by **Cat.1** (34%). This suggests that **Cat.3** without an intramolecular hydrogen bond can lead to faster $\text{C}\text{--}\text{I}$ cleavage, because of the increased electron density on the O^- moiety and the thereby enhanced halogen bonding. The quantitative electrostatic potential (ESP) analyses carried out using the Multiwfn 3.8 program^{51–53} show that the most negative point on the ESP map is around the O^- moiety in each catalyst and the ESP_{min} of **Cat.1** (-48.98 kcal/mol) is much larger than that of **Cat.3** (-55.71 kcal/mol), supporting the lower electron density on the O^- moiety of **Cat.1** than that for **Cat.3** (Figure 3). In addition, the DFT calculations indicate that the addition

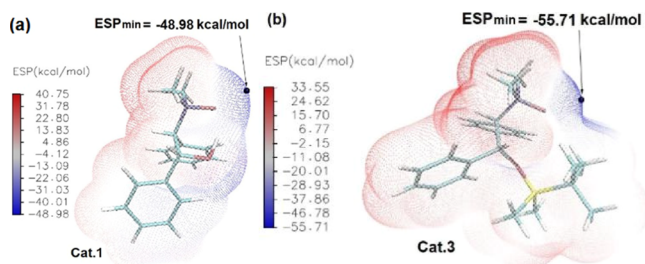


Figure 3. Color mapped isosurface graph of ESP of (a) **Cat.1** and (b) **Cat.3** generated with Multiwfn 3.8 program^{51,52} together with the visual MD program.⁵³

of **Cat.3** reduces the dissociation energy of $\text{MMA}\text{--}\text{I}$ from 31.3 to 26.3 kcal/mol (Scheme S1), which is lower than that by **Cat.1** (29.9 kcal/mol). These studies indicate that, compared with **Cat.1** bearing an intramolecular hydrogen bond, **Cat.3** is more conducive for promoting the formation of the radical, but gives a lower monomer conversion in the polymerizations targeting a high DP. This should be related to the predominant deactivator species, the efficiency of deactivation, and the preservation of “livingness”.

Formation of the $\text{I}_2/\text{Cat.1}$ Complex. UV–vis absorption spectroscopic analysis (Figure 4a) shows that, under irradiation, the absorption peak intensity of the polymerization system is gradually enhanced, and the shape is greatly changed, which centers at 365 and 297 nm and perfectly matches that for the $\text{I}_2/\text{Cat.1}$ mixture. Notably, compared with I_2 alone at the same concentration, the $\text{I}_2/\text{Cat.1}$ mixture exhibits an absorption peak with a much higher intensity and different

shape, indicating the complexation of I_2 with **Cat.1**. These results suggest that I^\cdot complexed or captured by **Cat.1** is so active that it tends to recombine with another one to generate the $\text{I}_2/\text{Cat.1}$ complex in the polymerization medium, as confirmed by a very fast color variation (within 10 min) from colorless to yellowish brown of the polymerization system (Figure 4a). Thus, the $\text{I}_2/\text{Cat.1}$ complex gradually accumulates during the polymerization process and enhances the light absorption intensity of the reaction system. In addition, the $\text{I}_2/\text{Cat.1}$ complex contributes to a wide visible light wavelength range extended to about 600 nm, so polymerizations are highly efficient mainly under visible light irradiation. The optimized structures of the complexes $\text{I}_2\cdots\text{Cat.1}$ and $\text{I}_2\cdots(\text{Cat.1})_2$ by DFT calculations show $\text{I}\cdots\text{O}$ distances of 2.60 and 2.83 Å (Figure 4b), respectively, suggesting the complexation and supporting the above deductions.^{54,55}

Identification of the Predominant Deactivator by DFT Calculations. Subsequently, DFT calculations of the deactivation process were performed.^{18,29,54} Figure 4c shows the energy profiles of reactions 3–5. As the ΔG_3 value for **Cat.1** is calculated to be -15.6 kcal/mol , reaction 3 proceeds exothermically so that the reaction of the two I^\cdot -catalyst radicals results in readily forming $\text{I}_2\cdots(\text{Cat.1})_2$. $\text{I}_2\cdots(\text{Cat.1})_2$ subsequently releases one catalyst molecule to generate $\text{I}_2\cdots\text{Cat.1}$ since reaction 4 is also greatly exothermic by 8.7 kcal/mol. Reaction 5, which releases the second catalyst to generate I_2 and **Cat.1**, is slightly exothermic ($\Delta G_5 = -0.2\text{ kcal/mol}$). These results indicate that among the possible four deactivators, $\text{I}_2\cdots\text{Cat.1}$ and I_2 are predominantly accumulated during the polymerization, which is consistent with the results of the UV–vis absorption analysis. When **Cat.3** was employed, the processes of generating $\text{I}_2\cdots(\text{Cat.3})_2$ and $\text{I}_2\cdots\text{Cat.3}$ are also exothermic, but the reaction 5 of generating I_2 is endothermic ($\Delta G_5' = 4.4\text{ kcal/mol}$). Therefore, $\text{I}_2\cdots\text{Cat}$ rather than I_2 should be a predominant deactivator for the **Cat.3** system. The work of C. Laurence et al. indicated that there is a satisfactory relationship between the ESP_{min} (electron density) of the Lewis base (B) and the equilibrium constant to form the $\text{B}\cdots\text{I}_2$ complex.⁵⁶ As mentioned above (Figure 3), we found that the ESP_{min} of **Cat.1** (-48.98 kcal/mol) is much larger than that of **Cat.3** (-55.71 kcal/mol), which corresponds to a weaker halogen bonding between **Cat.1** and I_2 . These studies confirm that the intramolecular hydrogen bond in **Cat.1** facilitates the release of the catalyst (activator) and I_2 , due to the reduced electron density on the O^- moiety and the thereby weakened halogen bonding.

DFT Calculations on the Deactivation Process. Reaction 6 plays an important role in the deactivation process due to the accumulation of $\text{I}_2\cdots\text{Cat}$. for both **Cat.1** and **Cat.3**. The energy barrier ΔG_6^\ddagger for **Cat.1** is small (13.9 kcal/mol), and thus the reaction can readily proceed (Figure 4d). The reaction is calculated to be exothermic ($\Delta G_6 = -5.6\text{ kcal/mol}$). The deactivation process with **Cat.3** is not so favorable as that by **Cat.1**, both dynamically and thermally ($\Delta G_6^{\ddagger'} = 15.3\text{ kcal/mol}$, $\Delta G_6' = -4.7\text{ kcal/mol}$). In addition, in the **Cat.1** system, I_2 is another predominant deactivator. The DFT calculation suggests that the deactivation by I_2 is more efficient, as it is barrierless (for details, please see the Supporting Information) and thermally feasible ($\Delta G_7 = -4.1\text{ kcal/mol}$). As shown in Figure S13, the energy profiles of reactions 3–6 by **Cat.4** are very similar to those using **Cat.3**. This is consistent with their very comparable catalytic performance in photo-RCMP. Through in situ NMR experiments (Figure S8), it is found

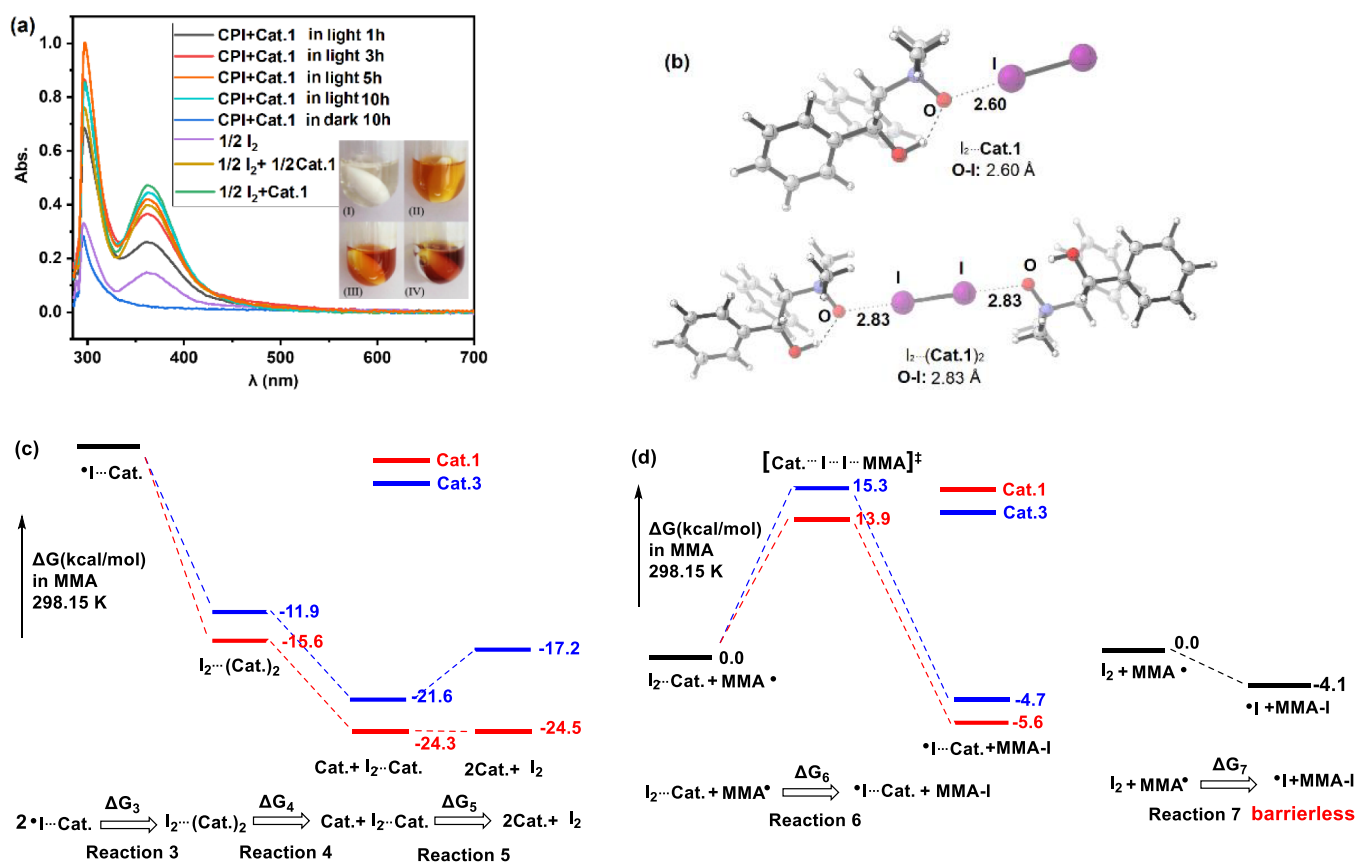


Figure 4. (a) UV-vis absorption spectra of bulk polymerization systems by Cat.1; the systems were diluted with MMA by 200 times before analysis (with the original CPI and Cat.1 concentration of 47.0 and 23.5 mM, respectively). Inset shows color variation of the polymerization system after 0 min (I), 10 min (II), 1 h (III), and 10 h (IV) (run 2, Table 1). (b) Optimized structures of $I_2 \cdot \text{Cat.1}$ and $I_2 \cdot (\text{Cat.1})_2$ complexes by DFT calculations. Free energy profiles of reactions 3–5 (c) and 6–7 (d).

that in the system of CPI with Cat.3 and Cat.4, under irradiation, only ca. 54 and 45% of CPI is retained after 4 h, respectively. By contrast, under the same conditions, ca. 78% of CPI is intact in the system with Cat.1, indicating the more reversible radical generation and more effective deactivation by Cat.1 than those by Cat.3 and Cat.4, and demonstrating the intramolecular hydrogen bond effects on the deactivation process.

Hydrogen Bond Effect Based on Modifying Electron Density. As experimentally observed and theoretically supported by DFT calculations, the “hydrogen bond effect” is based on modifying the electron density of the O^- moiety in N-oxide via H-bonding, which affect the release of I_2 from the $I_2 \cdot \text{Cat.}$ complex and thereby the controllability of the polymerization. In another way, Goto and co-workers optimized the catalytic performance of pyridine N-oxides based on adjusting the electron density of the O^- moiety by introducing different substituents,¹⁸ although these pyridine N-oxides are unable to give high-molecular-weight polymers with narrow distribution. Two other amino alcohol N-oxides (Cat.5 and Cat.6, Table S5) were also synthesized. Compared with Cat.1, Cat.5 has higher steric hindrance but similar electron density around the catalytic center (ESP analyses in Figures 3a and S13a). Cat.1 and Cat.5 obtain very similar results for the polymerizations whether targeting DP as 200 or 5000 (runs 1–4, Table S5). Cat.6 is an analog of Cat.1, with one phenyl replaced by a benzyl group, which weakens the intramolecular H-bonding and increases the electron density of the O^- moiety

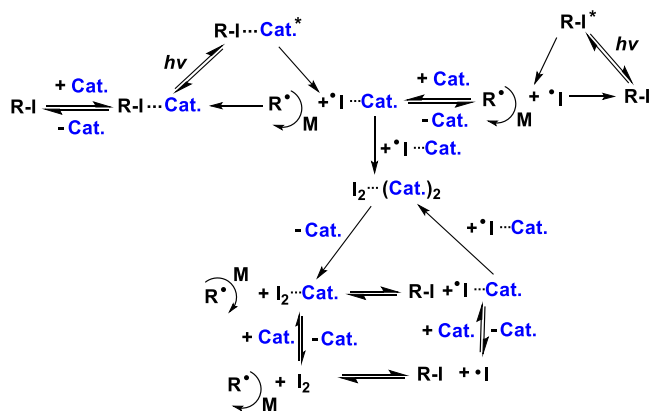
(ESP analyses in Figures 3a and S13b). With the $DP_{\text{target}} = 200$, Cat.6 achieves similar MMA polymerization results as Cat.1 (run 5, Table S). In the synthesis of high-molecular-weight PMMA ($DP_{\text{target}} = 5000$), Cat.6 affords much worse controllability on the polymerization ($D = 1.83$) than Cat.1 (run 11, Table 1 versus runs 6, Table S5). The polymerizations were also conducted employing pyridine N-oxides with different substituents as catalysts (Cat.4, Cat.7, and Cat.8). As shown in Tables 1 and S5, with $DP_{\text{target}} = 200$, all the three pyridine N-oxides can achieve efficient polymerizations of MMA with excellent controllability. For these three catalysts, the electron donating ability order of their substituents from low to high is Cat.8 (4-Ph) < Cat.7 (4-Me) < Cat.4 (4-piperidyl) (ESP analyses in Figure S13). While the controllability of the polymerization mediated by them is slightly improved with an opposite order: Cat.4 < Cat.7 < Cat.8. That is, the controllability of polymerization slightly improves with the decrease of electron density of the O^- moiety in the catalyst. The MMA polymerizations targeting DP as 5000 by these pyridine N-oxides (run 13, Table 1; runs 8 and 10, Table S5) obtain worse controllability and/or much lower conversions than those by amino alcohol N-oxides, but clearly indicate a similar rule, i.e., the lower the electron density of the O^- moiety, the more controllable the polymerization is in the synthesis of high-molecular-weight polymers. These results further highlight the advantages of our catalytic system in the synthesis of high-molecular-weight polymers and support our hypothesis of the hydrogen bond effect, which is

based on modifying the electron density of the O^- moiety in N-oxide via H-bonding.

These mechanism studies support our original conjecture and reveal that the intramolecular hydrogen bond of the N-oxide catalyst modifies the electron density of N-oxide, and thereby facilitates the regeneration of the catalyst (activator) and release of I_2 as a predominant effective regulator of radical concentration. This promotes the deactivation process, and thus lowers the radical concentration and suppresses the side-reactions, which prevents the loss of the livingness due to the extremely low concentration of deactivators. In addition, Cat.1 (activator) is regenerated in the process of releasing I_2 , thus ensuring rapid activation and finishing the catalytic cycle. Therefore, amino alcohol N-oxides that contain an intramolecular hydrogen bond achieve much higher polymerization efficiency within extended reaction times and much better controllability over high molecular weights compared with other studied catalysts.

Plausible Mechanism. Based on above studies, we proposed the mechanism by Cat.1 (Scheme 2). A complex

Scheme 2. Proposed Mechanism of Photo-RCMP by Cat.1



of dormant species and catalyst is initially formed. Subsequently, this complex is excited under irradiation, and the complex in the excited state dissociates to generate an alkyl radical and the complex $I \cdots \text{Cat.}$. This is the activation process that is widely recognized.^{18–28,48,57} Notably, under our experimental conditions, the radical trap experiments show that CPI could dissociate to produce radicals without the catalyst (Figure S4). In addition, the oligomer of MMA is produced (run 5, Table 1) in the absence of the catalyst, suggesting the direct photoexcitation of R–I (initiator/polymer–I). After being irradiated for 3 h, the absorption peak of I_2 could be clearly seen in the UV–vis spectrum (Figure S5) of CPI resolved in MMA with the same concentration as that of the bulk polymerization system (run 2, Table 1), further supporting the direct photoexcitation of R–I (initiator/polymer–I). Thus, there is a second activation process, that is, the decomposition of the excited R–I produces radicals, and the generated I^\cdot is complexed by the catalyst. Then, the formed alkyl radical (R^\cdot) triggered orderly chain propagation, while the iodine radical complexed by the catalyst recombines with another one to generate the complex $I_2 \cdots (\text{Cat.})_2$. The subsequent release of the catalyst leads to the generation of $I_2 \cdots \text{Cat.}$ as one deactivator. The intramolecular hydrogen bond promotes the dissociation of the $I_2 \cdots \text{Cat.}$ complex, regenerating the catalyst (activator) and releasing I_2

as another more effective deactivator. The deactivation reaction produces dormant species and I^\cdot or $I \cdots \text{Cat.}$. In subsequent reactions, the former (R–I) is activated to regenerate radicals, while the latter (I^\cdot or $I \cdots \text{Cat.}$) produces deactivators.

CONCLUSIONS

In summary, a novel and highly efficacious photo-RCMP system using amino alcohol N-oxide as the catalyst has been developed, allowing access to controlled high-molecular-weight polymers of different methacrylates ($M_n = 497–815$ kg/mol, $D < 1.5$) for the first time in photo-RCMP. The monomer conversion is nearly quantitative under simulated or natural sunlight irradiation. It is found that the intramolecular hydrogen bond in amino alcohol N-oxides plays a key role for the controllability and conversion in high- M_w -polymer synthesis. The insights of the hydrogen effects prove to modify the electron density of N-oxide and thereby facilitate the regeneration of the catalyst (activator) and release of I_2 as a predominant effective regulator of radical concentration by the studies of X-ray analysis, control experiments, DFT calculation, UV–vis absorption spectra, etc. The current work provides a new strategy for the development of highly efficient and well-controlled catalytic systems for organocatalytic photo-CRP, in particular to the synthesis of high-molecular-weight polymers.

ASSOCIATED CONTENT

Supporting Information

The Supporting Information is available free of charge at <https://pubs.acs.org/doi/10.1021/acscatal.2c03246>.

Experimental procedures, characterization, and DFT calculations (PDF)

Crystallographic information for Cat.1 (CIF)

AUTHOR INFORMATION

Corresponding Authors

Xiaoming Feng – Key Laboratory of Green Chemistry & Technology, Ministry of Education, College of Chemistry, Sichuan University, Chengdu 610064, P. R. China; orcid.org/0000-0003-4507-0478; Email: xmfeng@scu.edu.cn

Zhi-Pan Liu – Key Laboratory of Computational Physical Science (Ministry of Education), Shanghai Key Laboratory of Molecular Catalysis and Innovative Materials, Department of Chemistry, Fudan University, Shanghai 200433, China; orcid.org/0000-0002-2906-5217; Email: zpliu@fudan.edu.cn

Xiao-Yan Wang – State Key Laboratory of Organometallic Chemistry, Shanghai Institute of Organic Chemistry, Chinese Academy of Sciences, Shanghai 200032, China; orcid.org/0000-0002-6367-565X; Email: wangxiaoyan@sioc.ac.cn

Yong Tang – State Key Laboratory of Organometallic Chemistry, Shanghai Institute of Organic Chemistry, Chinese Academy of Sciences, Shanghai 200032, China; orcid.org/0000-0002-5435-9938; Email: tangy@sioc.ac.cn

Authors

Ya-Ning Li – State Key Laboratory of Organometallic Chemistry, Shanghai Institute of Organic Chemistry, Chinese Academy of Sciences, Shanghai 200032, China; School of Physical Science and Technology, ShanghaiTech University,

Shanghai 201210, China; University of Chinese Academy of Sciences, Beijing 100049, China

Sheng-Ye Zhang – State Key Laboratory of Organometallic Chemistry, Shanghai Institute of Organic Chemistry, Chinese Academy of Sciences, Shanghai 200032, China

Yang Ma – State Key Laboratory of Organometallic Chemistry, Shanghai Institute of Organic Chemistry, Chinese Academy of Sciences, Shanghai 200032, China; School of Physical Science and Technology, ShanghaiTech University, Shanghai 201210, China; University of Chinese Academy of Sciences, Beijing 100049, China

Yi-Jie Ding – State Key Laboratory of Organometallic Chemistry, Shanghai Institute of Organic Chemistry, Chinese Academy of Sciences, Shanghai 200032, China; School of Physical Science and Technology, ShanghaiTech University, Shanghai 201210, China; University of Chinese Academy of Sciences, Beijing 100049, China

Zhi-Hao Chen – State Key Laboratory of Organometallic Chemistry, Shanghai Institute of Organic Chemistry, Chinese Academy of Sciences, Shanghai 200032, China

Qiao-Ling Che – State Key Laboratory of Organometallic Chemistry, Shanghai Institute of Organic Chemistry, Chinese Academy of Sciences, Shanghai 200032, China; School of Physical Science and Technology, ShanghaiTech University, Shanghai 201210, China; University of Chinese Academy of Sciences, Beijing 100049, China

Long Qin – State Key Laboratory of Organometallic Chemistry, Shanghai Institute of Organic Chemistry, Chinese Academy of Sciences, Shanghai 200032, China

Xiu-Li Sun – State Key Laboratory of Organometallic Chemistry, Shanghai Institute of Organic Chemistry, Chinese Academy of Sciences, Shanghai 200032, China; orcid.org/0000-0001-7470-8544

Xiaohua Liu – Key Laboratory of Green Chemistry & Technology, Ministry of Education, College of Chemistry, Sichuan University, Chengdu 610064, P. R. China; orcid.org/0000-0001-9555-0555

Complete contact information is available at:
<https://pubs.acs.org/10.1021/acscatal.2c03246>

Notes

The authors declare no competing financial interest.

ACKNOWLEDGMENTS

The authors are grateful for financial support by the National Natural Science Foundation of China (21901253 and U19B6001), Youth Innovation Promotion Association CAS (No. 2020259), and Shanghai Rising-Star Program (21QA1411200). The authors are very grateful to the research group of Prof. Xiaoming Feng for providing the N,N'-dioxides for the initial study.

REFERENCES

- (1) Chen, M.; MacLeod, M. J.; Johnson, J. A. Visible-Light-Controlled Living Radical Polymerization from a Trithiocarbonate Iniferter Mediated by an Organic Photoredox Catalyst. *ACS Macro Lett.* **2015**, *4*, 566–569.
- (2) Pan, X.; Fang, C.; Fantin, M.; Malhotra, N.; So, W. Y.; Peteanu, L. A.; Isse, A. A.; Gennaro, A.; Liu, P.; Matyjaszewski, K. Mechanism of Photoinduced Metal-Free Atom Transfer Radical Polymerization: Experimental and Computational Studies. *J. Am. Chem. Soc.* **2016**, *138*, 2411–2425.
- (3) Treat, N. J.; Fors, B. P.; Kramer, J. W.; Christianson, M.; Chiu, C.-Y.; Read de Alaniz, J.; Hawker, C. J. Controlled Radical Polymerization of Acrylates Regulated by Visible Light. *ACS Macro Lett.* **2014**, *3*, 580–584.
- (4) Anastasaki, A.; Nikolaou, V.; Zhang, Q.; Burns, J.; Samanta, S. R.; Waldron, C.; Haddleton, A. J.; McHale, R.; Fox, D.; Percec, V.; Wilson, P.; Haddleton, D. M. Copper(II)/tertiary amine synergy in photoinduced living radical polymerization: accelerated synthesis of omega-functional and alpha,omega-heterofunctional poly(acrylates). *J. Am. Chem. Soc.* **2014**, *136*, 1141–1149.
- (5) Theriot, J. C.; Lim, C.-H.; Yang, H.; Ryan, M. D.; Musgrave, C. B.; Miyake, G. M. Organocatalyzed atom transfer radical polymerization driven by visible light. *Science* **2016**, *352*, 1082–1086.
- (6) Pan, X.; Malhotra, N.; Simakova, A.; Wang, Z.; Konkolewicz, D.; Matyjaszewski, K. Photoinduced Atom Transfer Radical Polymerization with ppm-Level Cu Catalyst by Visible Light in Aqueous Media. *J. Am. Chem. Soc.* **2015**, *137*, 15430–15433.
- (7) Ma, Q.; Song, J.; Zhang, X.; Jiang, Y.; Ji, L.; Liao, S. Metal-free atom transfer radical polymerization with ppm catalyst loading under sunlight. *Nat. Commun.* **2021**, *12*, 429.
- (8) Xu, J.; Jung, K.; Atme, A.; Shanmugam, S.; Boyer, C. A robust and versatile photoinduced living polymerization of conjugated and unconjugated monomers and its oxygen tolerance. *J. Am. Chem. Soc.* **2014**, *136*, 5508–5519.
- (9) Jiang, K.; Han, S.; Ma, M.; Zhang, L.; Zhao, Y.; Chen, M. Precise Synthesis of Photoorganocatalyzed Reversible-Deactivation Alternating Copolymerization of Chlorotrifluoroethylene and Vinyl Ethers under Ambient Conditions: Facile Access to Main-Chain Fluorinated Copolymers. *J. Am. Chem. Soc.* **2020**, *142*, 7108–7115.
- (10) Debuigne, A.; Schoumacker, M.; Willet, N.; Riva, R.; Zhu, X.; Rutten, S.; Erome, C.; Detrembleur, C. New functional poly(N-vinylpyrrolidone) based (co)polymers via photoinitiated cobalt-mediated radical polymerization. *Chem. Commun.* **2011**, *47*, 12703–12705.
- (11) Miao, X.; Zhu, W.; Zhang, Z.; Zhang, W.; Zhu, X.; Zhu, J. Photo-induced cobalt-mediated radical polymerization of vinyl acetate. *Polym. Chem.* **2014**, *5*, 551–557.
- (12) Zhao, Y.; Yu, M.; Zhang, S.; Wu, Z.; Liu, Y.; Peng, C. H.; Fu, X. A well-defined, versatile photoinitiator (salen)Co-CO₂CH₃ for visible light-initiated living/controlled radical polymerization. *Chem. Sci.* **2015**, *6*, 2979–2988.
- (13) Nakamura, Y.; Arima, T.; Tomita, S.; Yamago, S. Photoinduced switching from living radical polymerization to a radical coupling reaction mediated by organotellurium compounds. *J. Am. Chem. Soc.* **2012**, *134*, 5536–5539.
- (14) Yamago, S.; Ukai, Y.; Matsumoto, A.; Nakamura, Y. Organotellurium-Mediated Controlled/Living Radical Polymerization Initiated by Direct C-Te Bond Photolysis. *J. Am. Chem. Soc.* **2009**, *131*, 2100–2101.
- (15) Benedikt, S.; Moszner, N.; Liska, R. Benzoyl Phenyltelluride as Highly Reactive Visible-Light TERP-Reagent for Controlled Radical Polymerization. *Macromolecules* **2014**, *47*, 5526–5531.
- (16) Gong, H.; Gu, Y.; Zhao, Y.; Quan, Q.; Han, S.; Chen, M. Precise Synthesis of Ultra-High-Molecular-Weight Fluoropolymers Enabled by Chain-Transfer-Agent Differentiation under Visible-Light Irradiation. *Angew. Chem., Int. Ed.* **2020**, *59*, 919–927.
- (17) Corbin, D. A.; Miyake, G. M. Photoinduced Organocatalyzed Atom Transfer Radical Polymerization (O-ATRP): Precision Polymer Synthesis Using Organic Photoredox Catalysis. *Chem. Rev.* **2022**, *122*, 1830–1874.
- (18) Xu, H.; Wang, C.-G.; Lu, Y.; Goto, A. Pyridine N-Oxide Catalyzed Living Radical Polymerization of Methacrylates via Halogen Bonding Catalysis. *Macromolecules* **2019**, *52*, 2156–2163.
- (19) Wang, C.-G.; Chen, C.; Sakakibara, K.; Tsujii, Y.; Goto, A. Facile Fabrication of Concentrated Polymer Brushes with Complex Patterning by Photocontrolled Organocatalyzed Living Radical Polymerization. *Angew. Chem., Int. Ed.* **2018**, *57*, 13504–13508.

- (20) Ohtsuki, A.; Goto, A.; Kaji, H. Visible-Light-Induced Reversible Complexation Mediated Living Radical Polymerization of Methacrylates with Organic Catalysts. *Macromolecules* **2013**, *46*, 96–102.
- (21) Ohtsuki, A.; Lei, L.; Tanishima, M.; Goto, A.; Kaji, H. Photocontrolled Organocatalyzed Living Radical Polymerization Feasible over a Wide Range of Wavelengths. *J. Am. Chem. Soc.* **2015**, *137*, 5610–5617.
- (22) Tian, C.; Wang, P.; Ni, Y.; Zhang, L.; Cheng, Z.; Zhu, X. Photocontrolled Iodine-Mediated Reversible-Deactivation Radical Polymerization: Solution Polymerization of Methacrylates by Irradiation with NIR LED Light. *Angew. Chem., Int. Ed.* **2020**, *59*, 3910–3916.
- (23) Ni, Y.; Zhang, L.; Cheng, Z.; Zhu, X. Iodine-mediated reversible-deactivation radical polymerization: a powerful strategy for polymer synthesis. *Polym. Chem.* **2019**, *10*, 2504–2515.
- (24) Goto, A.; Ohtsuki, A.; Ohfujii, H.; Tanishima, M.; Kaji, H. Reversible generation of a carbon-centered radical from alkyl iodide using organic salts and their application as organic catalysts in living radical polymerization. *J. Am. Chem. Soc.* **2013**, *135*, 11131–11139.
- (25) Yang, H. J.; Wang, Z. R.; Zheng, Y. L.; Huang, W. Y.; Xue, X. Q.; Jiang, B. B. Synthesis of highly branched polymers by reversible complexation-mediated copolymerization of vinyl and divinyl monomers. *Polym. Chem.* **2017**, *8*, 2137–2144.
- (26) Wang, Y.-A.; Shi, Y.; Fu, Z.; Yang, W. Hexamethylphosphoramide as a highly reactive catalyst for the reversible-deactivation radical polymerization of MMA with an in situ formed alkyl iodide initiator. *Polym. Chem.* **2017**, *8*, 6073–6085.
- (27) Bai, L.; Zhang, L.; Pan, J.; Zhu, J.; Cheng, Z.; Zhu, X. Developing a Synthetic Approach with Thermoregulated Phase-Transfer Catalysis: Facile Access to Metal-Mediated Living Radical Polymerization of Methyl Methacrylate in Aqueous/Organic Biphasic System. *Macromolecules* **2013**, *46*, 2060–2066.
- (28) Ni, Y.; Tian, C.; Zhang, L.; Cheng, Z.; Zhu, X. Photocontrolled Iodine-Mediated Green Reversible-Deactivation Radical Polymerization of Methacrylates: Effect of Water in the Polymerization System. *ACS Macro Lett.* **2019**, *8*, 1419–1425.
- (29) Goto, A.; Sanada, S.; Lei, L.; Hori, K. Theoretical and Experimental Studies on Elementary Reactions in Living Radical Polymerization via Organic Amine Catalysis. *Macromolecules* **2016**, *49*, 2511–2517.
- (30) Chen, Z.-H.; Wang, X.-Y.; Sun, X.-L.; Li, J.-F.; Zhu, B.-H.; Tang, Y. Highly efficient atom transfer radical polymerization system based on the SaBOX/copper catalyst. *Macromolecules* **2019**, *52*, 9792–9798.
- (31) Chen, Z. H.; Ma, Y.; Wang, X.-Y.; Sun, X.-L.; Li, J.-F.; Zhu, B.-H.; Tang, Y. Winning strategy for iron-based ATRP using in situ generated iodine as a regulator. *ACS Catal.* **2020**, *10*, 14127–14134.
- (32) Wang, X.-Y.; Sun, X.-L.; Wang, F.; Tang, Y. SaBOX/copper catalysts for highly syndio-specific atom transfer radical polymerization of methyl methacrylate. *ACS Catal.* **2017**, *7*, 4692–4696.
- (33) Schaubach, S.; Wang, X.-Y.; Li, J.-F.; Sun, X.-L.; Wang, R. S.; Tang, Y. Yb(NTf₂)₃/HFIP induced high isotacticity in atom transfer radical polymerization of methyl methacrylate. *Polym. Chem.* **2018**, *9*, 4711–4715.
- (34) Wang, X.-Y.; Sun, X.-L.; Chen, Z.-H.; Wang, F.; Wang, R. S.; Tang, Y. Highly efficient access to well-defined linear polymers with substantial vinyl pendants via ATRP of divinyl monomers. *Polym. Chem.* **2018**, *9*, 4309–4315.
- (35) Wang, X.-Y.; Chen, Z.-H.; Sun, X.-L.; Tang, Y. Low temperature effect on ATRP of styrene and substituted styrenes enabled by SaBOX ligand. *Polymer* **2019**, *178*, No. 121630.
- (36) Ma, Y.; Yang, H.-M.; Chen, Z.-H.; Li, Y.-N.; Li, J.-F.; Sun, X.-L.; Wang, X.-Y.; Tang, Y. Highly branched polymethacrylates prepared efficiently: brancher-directed topology and application performance. *Polym. Chem.* **2021**, *12*, 6606–6615.
- (37) O'Neil, I. A.; Miller, N. D.; Peake, J.; Barkley, J. V.; Low, C. M. R.; Kalindjian, S. B. The Novel Use of Proline Derived Amine Oxides in Controlling Amide Conformation. *Synlett* **1993**, *1993*, 515–518.
- (38) Liu, X.; Lin, L.; Feng, X. Chiral N,N'-dioxide ligands: synthesis, coordination chemistry and asymmetric catalysis. *Org. Chem. Front.* **2014**, *1*, 298.
- (39) Hu, X.; Tang, X.; Zhang, X.; Lin, L.; Feng, X. Catalytic asymmetric Nakamura reaction by gold(I)/chiral N,N'-dioxide-indium(III) or nickel(II) synergistic catalysis. *Nat. Commun.* **2021**, *12*, 3012.
- (40) Zhang, D.; Su, Z.; He, Q.; Wu, Z.; Zhou, Y.; Pan, C.; Liu, X.; Feng, X. Diversified Transformations of Tetrahydroindolizines to Construct Chiral 3-Arylindolizines and Dicarbofunctionalized 1,5-Diketones. *J. Am. Chem. Soc.* **2020**, *142*, 15975–15985.
- (41) Cope, A. C.; Foster, T. T.; Towle, P. H. Thermal Decomposition of Amine Oxides to Olefins and Dialkylhydroxylamines. *J. Am. Chem. Soc.* **1949**, *71*, 3929–3934.
- (42) Cope, A. C.; Towle, P. H. Rearrangement of Allyldialkylamine Oxides and Benzyl dimethylamine Oxide. *J. Am. Chem. Soc.* **1949**, *71*, 3423–3428.
- (43) Cope, A. C.; Pike, R. A.; Spencer, C. F. Cyclic Polyolefins. XXVII. cis- and trans-Cyclooctene from N,N-Dimethylcyclooctylamine¹. *J. Am. Chem. Soc.* **1953**, *75*, 3212–3215.
- (44) Cope, A. C.; Trumbull, E. R. Olefins from Amines: The Hofmann Elimination Reaction and Amine Oxide Pyrolysis. *Org. React.* **2011**, *11*, 317–493.
- (45) Cooper, N. J.; Knight, D. W. The reverse Cope cyclisation: a classical reaction goes backwards. *Tetrahedron* **2004**, *60*, 243–269.
- (46) Chiao, W.-B.; Saunders, W. H., Jr. Mechanisms of elimination reactions. 29. Deuterium kinetic isotope effects in eliminations from amine oxides. The consequences of nonlinear proton transfer. *J. Am. Chem. Soc.* **1978**, *100*, 2802–2805.
- (47) Kwart, H.; Brechbiel, M. Role of solvent in the mechanism of amine oxide thermolysis elucidated by the temperature dependence of a kinetic isotope effect. *J. Am. Chem. Soc.* **1981**, *103*, 4650–4652.
- (48) Chen, Z.-H.; Wang, X.-Y.; Tang, Y. Reversible Complexation Mediated Polymerization: An Emerging Type of Organocatalytic Controlled Radical Polymerization. *Polym. Chem.* **2022**, *13*, 2402–2419.
- (49) Liu, X.; Lin, L.; Feng, X. Chiral N,N'-Dioxides: New Ligands and Organocatalysts for Catalytic Asymmetric Reactions. *Acc. Chem. Res.* **2011**, *44*, 574–587.
- (50) Aralikatti, N. V. Vibrational spectra, structure, theoretical calculations of 3-Fluoro-4-Hydroxybenzaldehyde: with evidence of hydrogen bonding. *J. Mol. Struct.* **2018**, *1173*, 814–821.
- (51) Lu, T.; Chen, F. Multiwfn: A Multifunctional Wavefunction Analyzer. *J. Comput. Chem.* **2012**, *33*, 580–592.
- (52) Lu, T.; Chen, F. Quantitative Analysis of Molecular Surface Based on Improved Marching Tetrahedra Algorithm. *J. Mol. Graph. Model.* **2012**, *38*, 314–323.
- (53) Humphrey, W.; Dalke, A.; Schulten, K. V. M. D. Visual Molecular Dynamics. *J. Mol. Graph.* **1996**, *14*, 27–28.
- (54) Nizhnik, Y. P.; Sons, A.; Zeller, M.; Rosokha, S. V. Effects of Supramolecular Architecture on Halogen Bonding between Diiodine and Heteroaromatic N-Oxides. *Cryst. Growth Des.* **2018**, *18*, 1198–1207.
- (55) Puttreddy, R.; Topić, F.; Valkonen, A.; Rissanen, K. HalogenBonded Co-Crystals of Aromatic N-oxides: Polydentate Acceptors for Halogen and Hydrogen Bonds. *Crystals* **2017**, *7*, 214.
- (56) Laurence, C.; Graton, J.; Berthelot, M.; Ghomari, M. J. E. The Diiodine Basicity Scale: Toward a General Halogen-Bond Basicity Scale. *Chem. – Eur. J.* **2011**, *17*, 10431–10444.
- (57) Miao, R.; Wang, D.; Xiao, J.; Ma, J.; Xue, D.; Liu, F.; Fang, Y. Halogen bonding matters: visible light-induced photoredox catalyst-free aryl radical formation and its applications. *Phys. Chem. Chem. Phys.* **2020**, *22*, 10212–10218.